Orthogonal Time Frequency Space (OTFS) With Dual-Mode Index Modulation

Hang Zhao, Dongxuan He, Ziqi Kang, and Hua Wang, *Member, IEEE*

***Abstract*—Orthogonal time frequency space (OTFS) modulation has been proved to have better bit error rate (BER) performance over orthogonal frequency division multiplexing (OFDM) under high-mobility conditions. In this letter, a new transmission scheme, called OTFS with dual-mode index modulation (OTFS-DM-IM), is proposed to balance the transmission reliability and spectral efficiency. Moreover, a modified log-likelihood ratio (LLR) detector based on the minimum Hamming distance is designed for demodulation. Then, the theoretical BER analysis of the proposed OTFS-DM-IM is presented. Simulation results highlight the performance advantage of OTFS-DM-IM over classical OTFS and the existing OTFS systems based on index modulation (OTFS-IM), and also confirm the superiority of the modified LLR detector compared to maximum likelihood detector and conventional LLR detector.**

***Index Terms*—OTFS, dual-mode index modulation, OTFS-DM-IM, modified log-likelihood ratio detector.**

I. Introduction

RELIABLE communication in high-mobility scenarios has been receiving tremendous attention in the fifth generation (5G) and future mobile communication systems. Although orthogonal frequency division multiplexing (OFDM) modulation technique currently adopted in the fourth generation (4G) systems performs well in time-invariant frequency selective channels, it is susceptible to time-varying cases with high Doppler spread due to severe inter-carrier interference (ICI).

Recently, an emerging multicarrier modulation technique, called orthogonal time frequency space (OTFS), was proposed to cope with time-varying scenarios [1]. The main premise behind OTFS is to convert the time-varying channel into a two-dimensional (2D) quasi-time-invariant channel in the delay-Doppler domain. Accordingly, all information symbols can be multiplexed in the delay-Doppler domain and spread over the time-frequency domain. Therefore, full diversity can be achieved and exploited, leading to superior performance gains compared to OFDM [2], [3].

In 5G cellular networks, the explosively growing demand of data services puts forward higher requirements for spectral efficiency (SE). Following this trend, the novel concept of index modulation (IM) has been extended to OFDM in recent years. Several OFDM based index modulation schemes were proposed in [4]–[6], where subcarrier indices are regarded as a source of information to enhance the SE. Yet in aforementioned studies, only a portion of subcarriers is activated, inevitably resulting in the waste of precious spectral resource. To overcome this shortcoming, a dual-mode index modulation aided OFDM (DM-OFDM-CPA) was developed, where all subcarriers are activated and modulated by two different constellation alphabets to make full use of spectral resources [7], [8]. To further increase the achievable rate, space-time shift keying was introduced into OFDM-based index modulation [9], [10]. However, such methodologies mainly focus on the design of transmission over time-invariant channels but do not work robustly over time-varying channels, thus limiting its implementation to dynamic scenarios. To tackle this problem, an index modulation based OTFS system (OTFS-IM) was proposed, where indices information is transmitted by the combination of active and silent grids in the delay-Doppler domain [11]. Nevertheless, OTFS-IM only performs well in low order modulation, where throughput loss may happen due to the slice of inactive grids.

In this letter, we exploit the potential of OTFS with dual-mode index modulation (OTFS-DM-IM) to facilitate transmission in high-mobility scenarios. The main contributions of this correspondence are summarized as follows: 1) A new scheme called OTFS-DM-IM is proposed to achieve a better trade-off between the transmission reliability and SE in time-varying channels. 2) A minimum Hamming distance based modified log-likelihood ratio (LLR) detector is investigated to realize the detection of our proposed OTFS-DM-IM. 3) Based on pairwise error probability (PEP), the upper bound of BER for OTFS-DM-IM is mathematically derived. Simulation results validate the superiority of OTFS-DM-IM and reveal the promising performance of the modified LLR detector.

Notation: We let x, $\mathbf{x}$, and $\mathbf{X}$ represent scalar, vector, and matrix, respectively. The transpose and conjugate transpose of a matrix are denoted as $(\cdot)^{\mathrm{T}}$ and $(\cdot)^{\mathrm{H}}$. The integer floor function, the Dirac delta function, and the sign function are denoted as $\lfloor\cdot\rfloor$, $\delta(\cdot)$, and $sgn(\cdot)$, respectively. Circulant matrix with the first column of $\mathbf{x}$ is referred to $circ\{\mathbf{x}\}$, and diagonal matrix with the elements of $\mathbf{x}$ is defined as $diag\{\mathbf{x}\}$. $\otimes$ is Kronecker product operator. $\mathbf{I}_N$ denotes the identity matrix of size $N \times N$, and $\mathbf{F}_M$ represents the M-point discrete Fourier transform (DFT) matrix. Finally, $\mathbb{E}_{\mathbf{x}}\{\cdot\}$ denotes the expectation operation with respect to $\mathbf{x}$.

Manuscript received December 31, 2020; accepted January 19, 2021. Date of publication January 25, 2021; date of current version May 10, 2021. This work was supported in part by the National Key Research and Development Program of China under Grant 2020YFB1807900; in part by the Postdoctoral Science Foundation of China under Grant 2020M670332; and in part by the National Natural Science Foundation of China under Grant 61471037. The associate editor coordinating the review of this article and approving it for publication was J. Coon. *(Corresponding author: Dongxuan He.)*

Hang Zhao, Ziqi Kang, and Hua Wang are with the School of Information and Electronics, Beijing Institute of Technology, Beijing 100081, China (e-mail: 3120180847@bit.edu.cn; ziqikang@bit.edu.cn; wanghua@bit.edu.cn).

Dongxuan He is with the Beijing National Research Center for Information Science and Technology, Department of Electronic Engineering, Tsinghua University, Beijing 100084, China (e-mail: dongxuan_he@tsinghua.edu.cn).

Digital Object Identifier 10.1109/LWC.2021.3053981

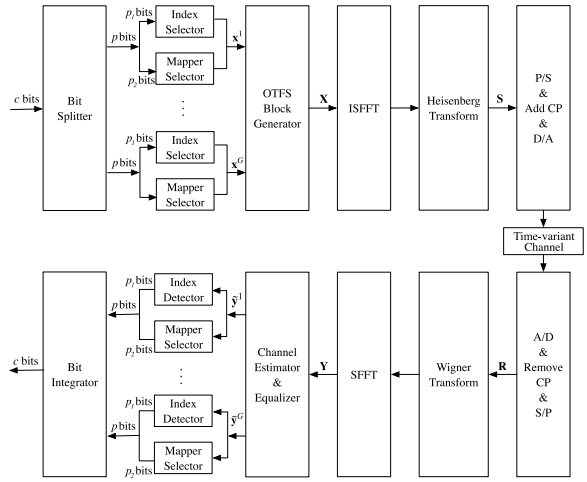

Fig. 1. Block diagram of the OTFS-DM-IM system.

TABLE I
A LOOK-UP TABLE FOR $L = 4$, $K = 2$ AND $p_1 = 2$

Index bits	Pattern	Index bits	Pattern
[0,0]	1 0 1 0	[1,1]	0 1 0 1
[0,1]	1 0 0 1	[1,0]	0 1 1 0

Note: 1 and 0 in the "Pattern" column of the table represent the modulation pattern $\mathcal{M}_A$ and $\mathcal{M}_B$, respectively.

II. System Model

We consider an OTFS-DM-IM system with *M* subcarriers and *N* symbols, where subcarrier spacing and symbol duration are Δf and *T*, respectively.

The block diagram of OTFS-DM-IM is depicted in Fig. 1. We assume a point-to-point scenario with a total of *c* bits for transmission. These *c* bits are split into *G* groups with *p* bits in each group. Each group of *p* bits is then divided into p_1 bits and p_2 bits, separately referred as index bits and information bits, to generate an OTFS subblock of length $L = NM/G$, where *NM* is the size of an OTFS frame. As shown in Fig. 1, the first p_1 bits are invoked by the index selector to determine the constellation alphabets of the remaining p_2 bits, i.e., $\mathcal{M}_A$ and $\mathcal{M}_B$ with sizes of M_A and M_B, respectively. Providing that *K* grids of the subblock are modulated with $\mathcal{M}_A$ and the other $(L - K)$ grids are modulated with $\mathcal{M}_B$, p_1 and p_2 can be calculated as $p_1 = \lfloor \log_2(C_L^K) \rfloor$ and $p_2 = K \log_2(M_A) + (L-K)\log_2(M_B)$ with C_L^K being the binomial coefficient. By means of the Gray-coded pairwise index mapping exemplified in Table I, the *g*-th subblock can be expressed as [12]

$$\mathbf{x}^g = [x^g(1), \ldots, x^g(\zeta), \ldots, x^g(L)]^{\mathrm{T}}, 1 \le g \le G, \quad (1)$$

where $x^g(\zeta) \in \{\mathcal{M}_A, \mathcal{M}_B\}$. Afterwards, all the subblocks are passed through the OTFS Block Generator to generate the delay-Doppler signal $\mathbf{X} \in \mathbb{C}^{M \times N}$.

Next, the practical OFDM-based OTFS structure is implemented [13]. The signal $\mathbf{X}$ is first converted to the time-frequency domain via the *inverse symplectic Fourier transform* (ISFFT), and then, the *Heisenberg transform* along with the pulse-shaping waveform $g_{\mathrm{tx}}(t)$ is adopted to yield a 2D transmitted signal $\mathbf{S} = \mathbf{G}_{\mathrm{tx}}\mathbf{F}_M^{\mathrm{H}}(\mathbf{F}_M\mathbf{X}\mathbf{F}_N^{\mathrm{H}}) = \mathbf{G}_{\mathrm{tx}}\mathbf{X}\mathbf{F}_N^{\mathrm{H}}$.[1] By column-wise vectorization of $\mathbf{S} \in \mathbb{C}^{M \times N}$, a one-dimensional (1D) transmitted signal $\mathbf{s} \in \mathbb{C}^{MN \times 1}$ can be obtained. To avoid inter-symbol interference (ISI) between OTFS blocks, a cyclic prefix (CP) is appended to the front of $\mathbf{s}$ before transmission.

The signal $\mathbf{s}$ is then transmitted over the time-varying channel with channel impulse response $h(\tau, \nu)$, which is characterized by delay τ and Doppler shift ν, given by [3]

$$h(\tau, \nu) = \sum_{i=1}^{P} h_i \delta(\tau - \tau_i)\delta(\nu - \nu_i), \quad (2)$$

where *P* is the number of propagation paths, h_i, τ_i and ν_i represent the channel gain, delay and Doppler shift for the *i*-th path, respectively. Accordingly, the delay and Doppler taps for the *i*-th path is defined as $\tau_i = \frac{l_i}{M\Delta f}$ and $\nu_i = \frac{k_i}{NT}$, where l_i and k_i are assumed to be integers.

After removing CP at the receiver, the received signal $\mathbf{r}$ can be rearranged as a matrix $\mathbf{R} \in \mathbb{C}^{M \times N}$. Then, the *Wigner transform* with the pulse-shaping waveform $g_{\mathrm{rx}}(t)$ and the *symplectic finite Fourier transform* (SFFT) are successively applied to get symbols $\mathbf{Y} = \mathbf{F}_M^{\mathrm{H}}(\mathbf{F}_M\mathbf{G}_{\mathrm{rx}}\mathbf{R})\mathbf{F}_N$ in the delay-Doppler domain. By vectorizing $\mathbf{Y}$, the signal $\mathbf{y} \in \mathbb{C}^{MN \times 1}$ is obtained, which can be grouped as

$$\begin{aligned}\mathbf{y}^g &= [y_{(g-1)L+1}, \ldots, y_{(g-1)L+\zeta}, \ldots, y_{(g-1)L+L}]^{\mathrm{T}} \\ &= [y^g(1), \ldots, y^g(\zeta), \ldots, y^g(L)]^{\mathrm{T}}, 1 \le g \le G. \end{aligned} \quad (3)$$

To eliminate ISI, channel estimation and equalization are adopted, where symbols in the *g*-th subblock turn to be $\tilde{\mathbf{y}}^g = [\tilde{y}^g(1), \ldots, \tilde{y}^g(\zeta), \ldots, \tilde{y}^g(L)]^{\mathrm{T}}$. Finally, $\tilde{\mathbf{y}}^g$ is sent to the detector to demodulate the index bits and information bits, which will be discussed in detail in Section III.

III. Detectors for OTFS-DM-IM

A. ML Detector

For an ML detector, all possible subblock realizations are considered by searching for all possible index patterns $\mathbf{\Psi}$ with its corresponding symbol combinations $\mathbf{S}_{\mathbf{\Psi}}$, which is mathematically formulated as

$$\left\{\hat{\Psi}, \hat{S}_{\hat{\Psi}}\right\} = \underset{\Psi \in \mathbf{\Psi}, S_\Psi \in \mathbf{S}_{\mathbf{\Psi}}}{\arg\min} \sum_{\zeta=1}^{L} |\tilde{y}^g(\zeta) - S_\Psi(\zeta)|^2, \quad (4)$$

where $\{\hat{\Psi}, \hat{S}_{\hat{\Psi}}\}$ represent the estimated index pattern and symbol constellation, and $S_\Psi(\zeta)$ denotes the ζ-th symbol in one legitimate symbol alphabet.

B. LLR Detector

Since the index pattern of the grid in the delay-Doppler domain is either 1 or 0, the logarithm of the ratio between the *a posteriori* probabilities of the grid modulated with $\mathcal{M}_A$ and that modulated with $\mathcal{M}_B$ can be utilized to identify the index pattern of the grid, which is formulated as

$$\gamma^g(\zeta) = \ln\left(\frac{\sum_{j=1}^{M_A} P(x^g(\zeta) = S_A(j)|\tilde{y}^g(\zeta))}{\sum_{j=1}^{M_B} P(x^g(\zeta) = S_B(j)|\tilde{y}^g(\zeta))}\right), \quad (5)$$

[1] $\mathbf{G}_{\mathrm{tx}}$ can be calculated as $diag\{g_{\mathrm{tx}}(0), g_{\mathrm{tx}}(T/M), \ldots, g_{\mathrm{tx}}((M-1)T/M)\}$. For rectangular waveforms, $\mathbf{G}_{\mathrm{tx}}$ reduces to the identity matrix $\mathbf{I}_M$.

with $S_A(j) \in \mathcal{M}_A$, $S_B(j) \in \mathcal{M}_B$. From (5), a positive $\gamma^g(\zeta)$ implies that the grid is more likely to be an $\mathrm{M_A}-\mathrm{ary}$ symbol. Therefore, the signs of $\gamma^g(\zeta)$ in the g-th subblock, calculated as $\bar{\boldsymbol{\gamma}}^g = [sgn(\gamma^g(1)), \ldots, sgn(\gamma^g(\zeta)), \ldots, sgn(\gamma^g(L))]^T$, can be viewed as the estimated index pattern, and subsequently, can be utilized to demodulate index bits.

However, the direct calculation of LLR values ignores the priori information of legitimate index patterns, probably leading to an illegitimate $\bar{\boldsymbol{\gamma}}^g$, which cannot be found in the given look-up table. Thereby, some measures need to be taken to address the occurrence of illegitimate index patterns.

1) Conventional LLR Detector: To tackle this problem, the conventional LLR detector directly decides the constellation alphabet of the grid, i.e., $\mathcal{M}_A$ or $\mathcal{M}_B$, according to the largest *K* LLR values [8]. To this end, the index bits can be recovered based on the given look-up table, and symbols of each grid can be demodulated by

$$\hat{x}^g(\zeta) = \begin{cases} \arg\min_{S_A(j)\in\mathcal{M}_A} |\tilde{y}^g(\zeta) - S_A(j)|^2, & \bar{\gamma}^g(\zeta) = 1, \\ \arg\min_{S_B(j)\in\mathcal{M}_B} |\tilde{y}^g(\zeta) - S_B(j)|^2, & \bar{\gamma}^g(\zeta) = 0. \end{cases} \tag{6}$$

2) Modified LLR Detector: Nevertheless, the performance of conventional LLR detector is poor under a high noise condition since grids with the largest *K* LLR values may still not correspond to one of the legitimate index patterns in the look-up table. Hereby, we propose a new modified algorithm based on the minimum Hamming distance to improve the detection performance as well as reducing the implementation complexity. The details are as follows.

Step 1: According to (5), calculate the LLR value of each grid in the subblock, and then, decide the corresponding signs to obtain initial estimated index pattern $\bar{\boldsymbol{\gamma}}^g$.

Step 2: Determine the Hamming distance between $\bar{\boldsymbol{\gamma}}^g$ and each legitimate index pattern, and find the possible legitimate index pattern alphabet $\mathcal{J}$ associated with the minimum Hamming distance d_{min}. In particular, the possible value of d_{min} is related to the subblock size *L*, i.e., $d_{min} \in \{0, \ldots, L/2\}$.

Step 3: Based on the value of d_{min}, the following three cases are demonstrated to identify the corresponding legitimate index pattern:

a) If $d_{min} = 0$, which means $\bar{\boldsymbol{\gamma}}^g$ is a legitimate index pattern, directly go to Step 4.

b) If $d_{min} = 1$, determine the position where the element of possible legitimate index patterns in $\mathcal{J}$ is different from that in $\bar{\boldsymbol{\gamma}}^g$ and reverse the element in $\bar{\boldsymbol{\gamma}}^g$ with the smaller LLR magnitude to match one of the legitimate index patterns. Then, go to Step 4.

c) If $d_{min} > 1$, reverse the element with the smallest LLR magnitude in $\bar{\boldsymbol{\gamma}}^g$ to reduce the minimum Hamming distance until $d_{min} = 1$. Then, go to Step 3.b.

Step 4: Demodulate the index bits based on the look-up table, and recover the information bits by the corresponding constellation demappers or give the soft output of bit likelihood ratio for further channel decoding.

Example: Based on Table I, we suppose the index bits [0,0] with index pattern [1 0 1 0] are transmitted. At the receiver, $\boldsymbol{\gamma}^g$ is calculated as $[6.01, -0.85, -1.17, -5.15]^T$ and $\bar{\boldsymbol{\gamma}}^g$ can be decided as [1 0 0 0] using Step 1. Next, the possible legitimate index pattern alphabet $\mathcal{J} = \{[1\,0\,1\,0], [1\,0\,0\,1]\}$ with $d_{min} = 1$ can be obtained according to Step 2. Following Step 3.b, since $|\gamma^g(3)| = 1.17 < |\gamma^g(4)| = 5.15$, the third element in $\bar{\boldsymbol{\gamma}}^g$ is reversed, and thus, $\bar{\boldsymbol{\gamma}}^g$ is corrected to [1 0 1 0]. Finally, recover the index bits and information bits through Step 4.

IV. Performance and Complexity Analysis

A. Analysis of SE

It is indicated that the SE of our proposed OTFS-DM-IM is determined by both the index bits n_{index} and the information bits n_{info}. Hence, it can be calculated as $\eta = (n_{\text{index}} + n_{\text{info}})/(NT)/(M\Delta f) = (\lfloor \log_2(C_L^K) \rfloor + K\log_2(M_A) + (L-K)\log_2(M_B))/L$. [2]

As a result, the SE gain of $((L-K)\log_2(M_B))/L$ can be achieved by our proposed OTFS-DM-IM compared to OTFS-IM with $\mathrm{M_A}$-ary QAM modulation [11]. For instance, when $L = 4$, $K = 2$, $M_A = 8$, and $M_B = 4$, the SE growth is up to 50%.

B. Analysis of BER

Based on PEP, the theoretical BER performance of OTFS-DM-IM with ML detection can be obtained. Specifically, according to Section II, the input-output relation of OTFS-DM-IM can be simplified as [13]

$$\mathbf{y} = (\mathbf{F}_N \otimes \mathbf{G}_{\text{rx}})\mathbf{H}(\mathbf{F}_N^{\text{H}} \otimes \mathbf{G}_{\text{tx}})\mathbf{x} + \mathbf{w}, \tag{7}$$

where $\mathbf{w}$ is zero mean additive noise with $\mathcal{CN}(0, N_0\mathbf{I}_{MN})$, and $\mathbf{H} \in \mathbb{C}^{MN\times MN}$ is the channel matrix, given by $\mathbf{H} = \sum_{i=1}^{P} h_i \mathbf{\Pi}^{l_i}\mathbf{\Delta}^{k_i}$, where $\mathbf{\Pi} = circ\{[0, 1, \ldots, 0]^{\text{H}}_{MN\times 1}\}$ is a circular delay matrix, and $\mathbf{\Delta} = diag\{z^0, z^1, \ldots, z^{MN-1}\}$ with $z = e^{\frac{j2\pi}{MN}}$ is a diagonal Doppler matrix.

The received signal in (7) can be rewritten as [14]

$$\mathbf{y} = \sum_{i=1}^{P} h_i(\mathbf{F}_N \otimes \mathbf{G}_{\text{rx}})\mathbf{\Pi}^{l_i}\mathbf{\Delta}^{k_i}(\mathbf{F}_N^{\text{H}} \otimes \mathbf{G}_{\text{tx}})\mathbf{x} + \mathbf{w} = \mathbf{\Phi}(\mathbf{x})\mathbf{h} + \mathbf{w}, \tag{8}$$

where $\mathbf{h} = [h_1, h_2, \ldots, h_P]^{\text{T}}$ is a $P \times 1$ vector with element $h_i \sim \mathcal{CN}(0, 1/P)$, and $\mathbf{\Phi}(\mathbf{x})$ is an $MN \times P$ concatenated matrix, given by

$$\mathbf{\Phi}(\mathbf{x}) = [\underbrace{\mathbf{\Xi}_1}_{MN\times MN}\ \underbrace{\mathbf{x}}_{MN\times 1} \mid \cdots \mid \underbrace{\mathbf{\Xi}_P}_{MN\times MN}\ \underbrace{\mathbf{x}}_{MN\times 1}], \tag{9}$$

with $\mathbf{\Xi}_i \triangleq (\mathbf{F}_N \otimes \mathbf{G}_{\text{rx}})\mathbf{\Pi}^{l_i}\mathbf{\Delta}^{k_i}(\mathbf{F}_N^{\text{H}} \otimes \mathbf{G}_{\text{tx}})$.

Subsequently, the conditional PEP (CPEP) for OTFS-DM-IM, which is defined as the probability of deciding $\hat{\mathbf{x}}$ when $\mathbf{x}$ is transmitted over a channel $\mathbf{h}$, can be given by [15]

$$\begin{aligned} \Pr(\hat{\mathbf{x}}|\mathbf{x}, \mathbf{h}) &= \mathbb{P}\Big(\|\mathbf{y} - \mathbf{\Phi}(\hat{\mathbf{x}})\mathbf{h}\|^2 < \|\mathbf{y} - \mathbf{\Phi}(\mathbf{x})\mathbf{h}\|^2 | \mathbf{x}, \mathbf{h}\Big) \\ &= Q\left(\sqrt{\frac{\boldsymbol{\delta}}{2N_0}}\right), \end{aligned} \tag{10}$$

where $Q(\cdot)$ is the Gaussian Q-function and

$$\boldsymbol{\delta} = \|[\mathbf{\Phi}(\hat{\mathbf{x}}) - \mathbf{\Phi}(\mathbf{x})]\mathbf{h}\|^2 = \mathbf{h}^{\text{H}}\mathbf{\Gamma}\mathbf{h}, \tag{11}$$

with $\mathbf{\Gamma} = (\mathbf{\Phi}(\hat{\mathbf{x}}) - \mathbf{\Phi}(\mathbf{x}))^{\text{H}}(\mathbf{\Phi}(\hat{\mathbf{x}}) - \mathbf{\Phi}(\mathbf{x}))$. Here, $\mathbf{\Gamma}$ can be decomposed as $\mathbf{U}\mathbf{\Lambda}\mathbf{U}^{\text{H}}$ for it is a Hermitian matrix, where $\mathbf{U}$

[2] Specifically, CP is not considered during the calculation of SE since the impact of CP is the same in all schemes.

TABLE II
DELAY PROFILE WITH $P = 5$ FOR SIMULATION

Path index (i)	1	2	3	4	5
Delay (τ_i), μs	0	2.08	4.164	6.246	8.328

is unitary and $\mathbf{\Lambda} = diag\{\lambda_1, \ldots, \lambda_P\}$ with λ_i being the i-th eigenvalue of $\mathbf{\Gamma}$. Thus, (11) can be simplified as

$$\boldsymbol{\delta} = \tilde{\mathbf{h}}^{\mathrm{H}}\mathbf{\Gamma}\tilde{\mathbf{h}} = \sum_{l=1}^{r} \lambda_l |\tilde{h}_l|^2, \tag{12}$$

where $\tilde{\mathbf{h}} = \mathbf{U}^{\mathrm{H}}\mathbf{h}^{\mathrm{H}}$ with $\tilde{h}_l \sim \mathcal{CN}(0, 1/P)$, and r denotes the rank of $\mathbf{\Gamma}$. Substituting (12) into (10), the corresponding unconditional PEP (UPEP) can be calculated as

$$\begin{aligned} \Pr(\hat{\mathbf{x}}|\mathbf{x}) &= \mathbb{E}_{\mathbf{h}}[Pr(\hat{\mathbf{x}}|\mathbf{x}, \mathbf{h})] \\ &= \mathbb{E}_{\mathbf{h}}\left[Q\left(\sqrt{\frac{\sum_{l=1}^{r} \lambda_l |\tilde{h}_l|^2}{2N_0}} \right) \right]. \end{aligned} \tag{13}$$

In light of the Chernoff bound, the upper bound on the average bit error probability (ABEP) can be written as [15]

$$P_e = \frac{1}{cn_{\mathbf{x}}} \sum_{\mathbf{x}} \sum_{\hat{\mathbf{x}} \neq \mathbf{x}} \Pr(\hat{\mathbf{x}}|\mathbf{x}) e(\hat{\mathbf{x}}, \mathbf{x}) \tag{14}$$

$$\leq \frac{1}{cn_{\mathbf{x}}} \sum_{\mathbf{x}} \sum_{\hat{\mathbf{x}} \neq \mathbf{x}} e(\hat{\mathbf{x}}, \mathbf{x}) \prod_{l=1}^{r} \frac{1}{1 + \frac{\lambda_l}{4N_0 P}}, \tag{15}$$

where $n_{\mathbf{x}}$ is the number of the possible realizations of $\mathbf{x}$, and $e(\hat{\mathbf{x}}, \mathbf{x})$ represents the number of bit errors for the corresponding pairwise error events.

C. Analysis of Detector Complexity

In terms of computational complexity, the ML detector is on the order of $\mathcal{O}(2^{p_1} M_A^K M_B^{L-K})$ for each subblock, which increases exponentially with the subblock size L and modulation orders M_A, M_B. On the contrary, the computational complexity of LLR-based detectors is $\mathcal{O}(L(M_A + M_B))$, which is much lower than that of the ML detector. Moreover, the conventional LLR detector introduces additional search complexity of $\mathcal{O}(L^2)$ for comparison of LLR values, while the search complexity of the modified detector is reduced to $\mathcal{O}(L)$ by only processing the illegitimate index pattern and converting the comparison of specific LLR values to the calculation of Hamming distance between $\bar{\boldsymbol{\gamma}}^g$ and legitimate index patterns.

V. SIMULATION RESULTS

We consider a channel with $P = 5$ propagation paths, where the delay profile is defined in Table II [16], and the Doppler profile is given by $\nu_i = \nu_{max} \cos(\theta_i)$ with ν_{max} being the maximum Doppler shift and $\theta_i \sim U[-\pi, \pi]$ [3]. In all simulations, ν_{max} is set to be 1850 Hz for the UE speed of 500 km/h and carrier frequency of 4 GHz. In particular, perfect channel estimation is assumed, and the Gray-coded pairwise index mapping with $L = 4$, $K = 2$ shown in Table I is adopted. Moreover, the SEs with corresponding constellation alphabets are included in Table III, where the optimal amplitude ratio between two constellations is considered in dual-mode schemes to guarantee the optimal performance.

TABLE III
CONSTELLATION ALPHABET FOR DIFFERENT SES

SE (bps/Hz)	Scheme	Constellation
1.5	Single-mode IM	4QAM
	Dual-mode IM	BPSK / BPSK
2.5	Single-mode IM	16QAM
	Dual-mode IM	QPSK / QPSK
3	Classical	8PSK
	Dual-mode IM	8PSK / QPSK
4	Classical	16QAM
	Dual-mode IM	16PSK / 8PSK

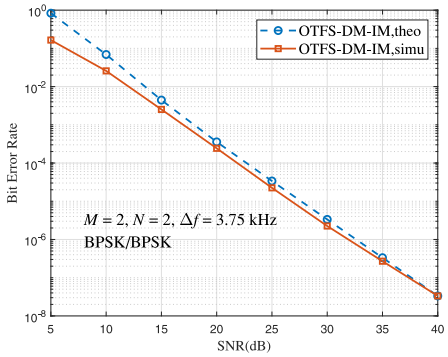

Fig. 2. BER performance of OTFS-DM-IM with spectral efficiency of 1.5 bps/Hz when $M = 2$, $N = 2$, and $\Delta f = 3.75$ kHz.

Firstly, the effectiveness of the derived BER upper bound of OTFS-DM-IM generated from (14) is examined in Fig. 2 with SE $= 1.5$ bps/Hz, $M = 2$, $N = 2$, and $\Delta f = 3.75$ kHz. It can be seen that the theoretical upper bound is gradually close to the simulation results with the increase of SNR. Particularly, when SNR is over 35 dB, the upper bound will precisely match the simulation points, thus validating the correctness of our derived upper bound.

In Fig. 3, we compare the BER performance of the proposed OTFS-DM-IM with that of OTFS-IM, DM-OFDM-CPA [8], classical OTFS, and classical OFDM when $M = 32$, $N = 32$, and $\Delta f = 15$ kHz. Among the comparison, minimum mean square error (MMSE) equalization and the ML detector are implemented in all systems. It can be seen from Fig. 3(a) that for the SE of 1.5 bps/Hz, compared to OTFS-IM, the proposed scheme has around 0.5 dB performance gain at the BER of 10^{-5}. This is because the dual-mode scheme of BPSK/BPSK and the single-mode scheme of 4QAM have almost the same robustness to noise and interference. Moreover, when SE is 2.5 bps/Hz, the proposed scheme achieves a larger performance gain compared to OTFS-IM, namely, more than 10 dB gains at the BER of 10^{-3}. This can be explained by the fact that OTFS-DM-IM only needs to employ QPSK/QPSK for reaching the SE of 2.5 bps/Hz, while a higher order modulation (i.e., 16QAM) has to be adopted in OTFS-IM, which is more sensitive to both noise and interference. Notably, DM-OFDM-CPA can not achieve satisfactory BER performance since the orthogonality of subchannels is impaired due to the time variation of the high-mobility channel.

Furthermore, in Fig. 3(b), compared to classical OTFS, the proposed OTFS-DM-IM has a nearly 1.7 dB performance gain at the BER of 10^{-3} with SE $= 3$ bps/Hz. This is because

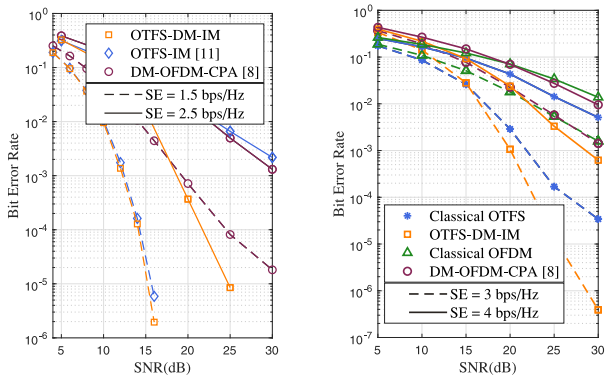

(a) SE = 1.5 bps/Hz, 2.5 bps/Hz (b) SE = 3 bps/Hz, 4 bps/Hz

Fig. 3. BER performance of OTFS-DM-IM, OTFS-IM, DM-OFDM-CPA, classical OTFS, and classical OFDM when $M = 32$, $N = 32$, and $\Delta f = 15$ kHz.

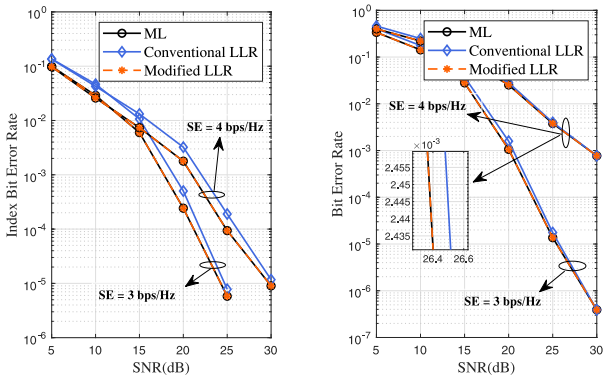

(a) index bits only (b) index bits + information bits

Fig. 4. BER performance of ML, conventional LLR, and the modified LLR detector in OTFS-DM-IM when $M = 32$, $N = 32$, and $\Delta f = 15$ kHz.

a higher order modulation (i.e., 8PSK) is adopted in classical OTFS to achieve the same SE as OTFS-DM-IM. When SE increases to 4 bps/Hz, a larger performance gain can be observed. Hereby, neither of classical OFDM and DM-OFDM-CPA can achieve good BER performance due to the loss of orthogonality of subchannels.

Finally, the index bit error rate (IER) and overall BER performance of OTFS-DM-IM with different detectors, including ML, conventional LLR, and the proposed modified LLR detector, are illustrated in Fig. 4. It is indicated in Fig. 4(a) that compared to the conventional LLR detector, the proposed modified LLR detector can attain 1.3 dB SIR-gain for IER $= 10^{-3}$ with SE of 3 bps/Hz, and can still achieve 1.1 dB SNR-gain for the same IER level with SE of 4 bps/Hz. As for the overall BER performance, it can be observed in Fig. 4(b) that the proposed modified LLR detector outperforms the conventional LLR detector in low and medium SNR regimes due to its higher detection accuracy of index bits. Although these two detectors have similar BER performance under high SNRs, the modified LLR detector imposes a lower search complexity. In addition, the modified LLR detector can achieve almost the same BER performance as the optimal ML detector in all SNR regimes, whilst greatly reducing the computational complexity.

VI. Conclusion

In this letter, we proposed a new transmission scheme called OTFS with dual-mode index modulation (OTFS-DM-IM). In this scheme, symbols mapped to the delay-Doppler domain are modulated with two different constellation alphabets to transmit additional index bits. At the receiver, a modified LLR detector based on the minimum Hamming distance was investigated to demodulate the received signals. Moreover, the theoretical BER upper bound was presented to give the benchmark of OTFS-DM-IM. Simulation results demonstrate that the proposed OTFS-DM-IM has better performance in terms of spectral efficiency and BER compared to classical OTFS and the existing OTFS-IM, and also reveal that the modified LLR detector with lower computational complexity can achieve almost the same performance as the ML detector.

References

[1] R. Hadani *et al.*, "Orthogonal time frequency space modulation," in *Proc. IEEE Wireless Commun. Netw. Conf. (WCNC)*, San Francisco, CA, USA, Mar. 2017, pp. 1–6.

[2] G. D. Surabhi, R. M. Augustine, and A. Chockalingam," "On the diversity of uncoded OTFS modulation in doubly-dispersive channels," *IEEE Trans. Wireless Commun.*, vol. 18, no. 6, pp. 3049–3063, Jun. 2019.

[3] P. Raviteja, K. T. Phan, Y. Hong, and E. Viterbo, "Interference cancellation and iterative detection for orthogonal time frequency space modulation," *IEEE Trans. Wireless Commun.*, vol. 17, no. 10, pp. 6501–6515, Oct. 2018.

[4] R. Abu-alhiga and H. Haas, "Subcarrier-index modulation OFDM," in *Proc. IEEE Int. Symp. Pers. Indoor Mobile Radio Commun.*, Tokyo, Japan, Sep. 2009, pp. 177–181.

[5] D. Tsonev, S. Sinanovic, and H. Haas, "Enhanced subcarrier index modulation (SIM) OFDM," in *Proc. IEEE GLOBECOM Workshops*, Houston, TX, USA, Dec. 2011, pp. 728–732.

[6] E. Başar, U. Aygölü, E. Panayırcı, and H. V. Poor, "Orthogonal frequency division multiplexing with index modulation," *IEEE Trans. Signal Process.*, vol. 61, no. 22, pp. 5536–5549, Nov. 2013.

[7] T. Mao, Z. Wang, Q. Wang, S. Chen, and L. Hanzo, "Dual-mode index modulation aided OFDM," *IEEE Access*, vol. 5, pp. 50–60, 2017.

[8] X. Zhang, H. Bie, Q. Ye, C. Lei, and X. Tang, "Dual-mode index modulation aided OFDM with constellation power allocation and low-complexity detector design," *IEEE Access*, vol. 5, pp. 23871–23880, 2017.

[9] M. I. Kadir, "Generalized space–time–frequency index modulation," *IEEE Commun. Lett.*, vol. 23, no. 2, pp. 250–253, Feb. 2019.

[10] S. Sugiura, T. Ishihara, and M. Nakao, "State-of-the-art design of index modulation in the space, time, and frequency domains: Benefits and fundamental limitations," *IEEE Access*, vol. 5, pp. 21774–21790, 2017.

[11] Y. Liang, L. Li, P. Fan, and Y. Guan, "Doppler resilient orthogonal time frequency space (OTFS) systems based on index modulation," in *Proc. IEEE Veh. Technol. Conf.*, Antwerp, Belgium, 2020, pp. 1–5.

[12] X. Li, H. Wang, N. Guan, and W. Lai, "A dual-mode index modulation scheme with gray-coded pairwise index mapping," *IEEE Commun. Lett.*, vol. 22, no. 8, pp. 1580–1583, Aug. 2018.

[13] P. Raviteja, Y. Hong, E. Viterbo, and E. Biglieri, "Practical pulse-shaping waveforms for reduced-cyclic-prefix OTFS," *IEEE Trans. Veh. Technol.*, vol. 68, no. 1, pp. 957–961, Jan. 2019.

[14] E. Biglieri, P. Raviteja, and Y. Hong, "Error performance of orthogonal time frequency space (OTFS) modulation," in *Proc. IEEE Int. Conf. Commun. Workshops*, Shanghai, China, 2019, pp. 1–6.

[15] D. Tse and P. Viswanath, *Fundamentals of Wireless Communication*. Cambridge, U.K.: Cambridge Univ. Press, 2005.

[16] M. K. Ramachandran and A. Chockalingam, "MIMO-OTFS in high-doppler fading channels: Signal detection and channel estimation," in *Proc. IEEE Global Commun. Conf.*, Abu Dhabi, UAE, 2018, pp. 206–212.